タイトル Title	Electrochemical Lithiation and Delithiation Properties of FeSi2/Si Composite Electrodes in Ionic-Liquid Electrolytes
著者 Auther(s)	Domi, Yasuhiro; Usui, Hiroyuki; Shindo, Yoshiko; Yodoya, Shuhei; Sato, Hironori; Nishikawa, Kei; Sakaguchi, Hiroki
掲載誌・巻号・ページ Citation	ELECTROCHEMISTRY , 88 (6) : 548 - 554
刊行日 Issue Date	2020
資源タイプ Resource Type	学術雑誌論文 / Journal Article
版区分 Resource Version	著者版 / Author
権利 Rights	(C) The Author(s) 2020. Published by ECSJ.
DOI	10.5796/electrochemistry.20-00091
URL	https://repository.lib.tottori-u.ac.jp/10185

Electrochemical Lithiation and Delithiation Properties of $FeSi_2$/Si Composite Electrodes in Ionic-Liquid Electrolytes

Yasuhiro Domi,[a,c] Hiroyuki Usui,[a,c] Yoshiko Shindo,[b,c] Shuhei Yodoya,[b,c] Hironori Sato,[b,c] Kei Nishikawa,[d] Hiroki Sakaguchi[a,c,*]

[a] Department of Chemistry and Biotechnology, Graduate School of Engineering, [b] Course of Chemistry and Biotechnology, Department of Engineering, Graduate School of Sustainability Science, and [c] Center for Research on Green Sustainable Chemistry, Tottori University, Minami 4–101, Koyama–cho, Tottori 680–8552, Japan

[d] International Center of Young Scientists, National Institute for Materials Science, 1–1 Namiki, Tsukuba 305–0044, Japan

* Corresponding authors:

Hiroki Sakaguchi

E–mail address: sakaguch@tottori-u.ac.jp

Tel/Fax: +81–857–31–5265

Abstract

We investigated the applicability of ionic-liquid electrolytes to $FeSi_2$/Si composite electrode for lithium-ion batteries. In conventional organic-liquid electrolytes, a discharge capacity of the electrode rapidly faded. In contrast, the electrode exhibited a superior cycle life with a reversible capacity of 1000 mA h $g(Si)^{-1}$ over 850 cycles in a certain ionic-liquid electrolyte. The difference in the cycle life was explained by surface film properties. In addition, the rate performance of the $FeSi_2$/Si electrode improved in another ionic-liquid electrolyte. Remarkably, lithiation of only Si in $FeSi_2$/Si composite electrode occurred whereas each $FeSi_2$- and Si-alone electrode alloyed with Li in the ionic-liquid electrolyte. $FeSi_2$ certainly covered the shortcomings of Si and the $FeSi_2$/Si composite electrode exhibited improved cycle life and rate capability compared to Si-alone electrode.

Keywords

lithium-ion battery; negative electrode; composite; ionic-liquid electrolyte;

Abstract Graphics

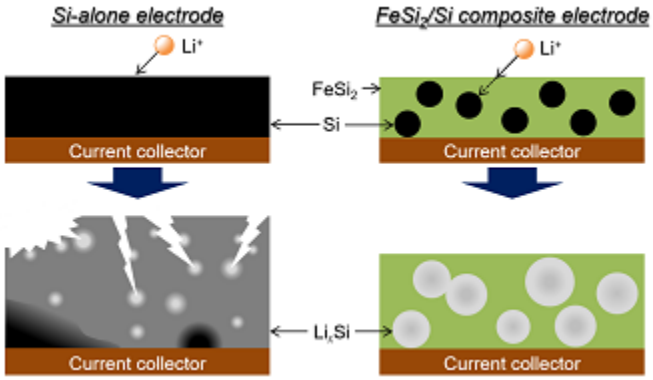

1. Introduction

Silicon (Si) electrode offer the promise of lithium-ion batteries (LIBs) with a high energy density due to its high theoretical capacity (3600 mA h g^{-1} for $Li_{15}Si_4$ phase).[1-4] However, the electrode typically show poor cycle lives due to their massive volume change of 280% upon complete lithiation at room temperature, generating high stress and large strain in the active material.[3,5] The strain leads to cracking and/or pulverization of Si, and then, the Si electrode disintegrates and the capacity fading occurs. Si has additional drawbacks, such as low electronic conductivity and a low Li^+ diffusion coefficient.[6-8]

To solve these issues, many research groups have put in a lot of work on construction of new active materials including the following: coating of Si with conductive materials to reduce the electrical resistivity;[9-11] synthesizing nanostructured Si materials that accommodate volume expansion;[12-14] pre-lithiation of Si to decrease the relative volume change in Si during charge/discharge reactions;[15,16] doping of Si with impurities including phosphorous (P), boron (B) and so on, to improve its electronic conductivity and/or change its properties, such as its phase transition, crystallinity morphology, and Li^+ diffusion;[8,17-19] and preparing composite electrodes that consisted of elemental Si and binary or ternary transition metal silicide to cover the shortcomings of Si.[20-24] We have reported that four properties are mainly required for composite materials as follows: (1) mechanical properties suitable for relaxation of the stress generating from Si, (2) high electronic conductivity, (3) moderate reactivity with Li^+, and (4) High thermodynamic stability.[20,25,26]

Electrolyte also contributes to improve the performance and safety of rechargeable batteries.[27-33] Because higher energy density of the batteries leads to an increase in risk of burning, nonflammable

electrolytes are an important concern regarding the safety.[34-36] Ionic-liquids have superior physicochemical properties as electrolyte solvents: ignorable vapor pressure, non-flammability, and wide electrochemical window.[37-40] Thus, the ionic-liquids are attractive as electrolyte solvents. We have demonstrated that Si-based electrodes offer greater lithiation/delithiation properties in some ionic-liquid electrolytes compared to that in conventional organic-liquid electrolytes in addition to the safety.[8,41-47] We have investigated the effect of cation structure of *N*-methyl-*N*-propylpyrrolidinium bis(trifluoromethanesulfonyl)amide (TFSA)-based ionic-liquid electrolyte on the electrochemical performance of Si-based electrodes.[48] 1-((2-methoxyethoxy)methyl)-1-methylpiperidinium (PP1MEM) cation played a role reducing the interaction between Li ion and TFSA anions, and Li^+ transfer at the electrode−electrolyte interface in PP1MEM-TFSA was remarkably improved compared with 1-hexyl-1-methylpiperidinium (PP16)-TFSA; the introduction of ether functional group into cation is valid to enhance the electrode property. We have also reported the influence of the anions (TFSA, bis(fluorosulfonyl)amide (FSA), and BF_4^-) in PP1MEM-based ionic-liquid electrolyte on the electrochemical performance; long cycle life and high rate performance were obtained in PP1MEM-FSA.[43]

In the present study, we investigate the applicability of ionic-liquid electrolytes to $FeSi_2$/Si composite electrodes for LIBs. We selected the $FeSi_2$/Si composite because ferrosilicon (Fe-Si) is used for deoxidation and desulfurization from molten steel in a steel process and inexpensive than metal grade Si: if we can divert the Fe-Si to an active material for negative electrode in LIBs, the cost of next-generation LIBs can be kept down. We used 1 mol dm^{-3} (M) lithium bis(fluorosulfonyl)amide (LiFSA)

dissolved in *N*-methyl-*N*-propylpyrrolidinium bis(fluorosulfonyl)amide (Py13-FSA) or 1-ethyl-3-methylimidazolium bis(fluorosulfonyl)amide (EMI-FSA) as the electrolytes because most Si-based electrodes exhibited a superior performance in them.[8,41-47] We also discuss the reaction behavior of $FeSi_2$/Si composite electrodes compared to that of Si- and $FeSi_2$-alone electrodes.

2. Experimental

Materials and Electrode Preparation. —— $FeSi_2$/Si powder (56/44 wt.%, Elkem ASA, HP FeSi65) and commercial Si powder (FUJIFILM Wako Pure Chemical Corporation, Ltd., 99.9%) were employed as the active materials. $FeSi_2$/Si (42/58 wt.%, Elkem ASA, HP FeSi75) which differs in composition was also used. $FeSi_2$ powder was synthesized by mechanical alloying (MA) method and its preparation procedure was described in our previous paper.[45] The $FeSi_2$/Si powder was characterized by X-ray diffraction (XRD, Ultima IV, Rigaku) and particle size distribution analyzer (SALD-2300, Shimazu).

Si-based electrodes were prepared by a gas deposition (GD) method without any conductive agent and/or binder. Copper foil (thickness: 20 μm, 99.9%) was used as a current collector. Ar and He carrier gases were used for preparation of Si and $FeSi_2$ or $FeSi_2$/Si electrodes, respectively. The weight of deposited active material on current collector was 30±2 μg. Other detailed GD conditions were previously reported.[8,19,49]

Charge-Discharge Testing. —— Galvanostatic charge-discharge testing were carried out with a 2032-type coin cell. The working electrode was the fabricated GD electrode. A Li metal sheet (thickness: 1

mm, 99.90%, Rare Metallic Co., Ltd.) and a glass fiber filter (Whatman GF/A) were used as the counter electrode and the separator. The ionic-liquid electrolyte used was 1 M LiFSA dissolved in Py13-FSA or EMI-FSA. LiFSA and above ionic-liquids were purchased from Kishida Chemical Co., Ltd. and Kanto Chemical Co., Inc., respectively. For comparison, 1 M lithium bis(trifluoromethanesulfonyl)amide (LiTFSA) dissolved in propylene carbonate (PC, Kishida Chemical Co., Ltd.) and 1 M LiFSA/PC were employed as a conventional organic-liquid electrolyte. Figure S1 shows chemical structure of Li-salts, ionic-liquids, and organic-liquid used in this study. The electrolyte preparation and cell assembly were performed in an Ar-filled glovebox (Miwa MFG, DBO-2.5LNKP-TS) with a dew point below –100ºC and an oxygen content less than 1 ppm.

The charge-discharge testing was carried out using an electrochemical measurement system (HJ-1001SD8, Hokuto Denko Co., Ltd.) in the potential range between 0.005 and 2.000 V vs. Li^+/Li at 303 K with a charge capacity limit of 1000 mA h $g(Si)^{-1}$ unless otherwise noted. The charge capacity was limited by controlling the charging time (about 42 min, 0.4*C*), while the discharging time was not limited and the cut off voltage was set at 2.000 V. The current density was set at 0.36 A $g(Si)^{-1}$ (0.1*C*) during the first cycle and 1.44 A $g(Si)^{-1}$ (0.4*C*) during the subsequent cycles unless otherwise stated. The rate capability was also investigated at *C*-rates from 0.1 to 50*C*.

Scanning Electron Microscopy. —— The cell was disassembled in the glovebox after the charge-discharge testing and the electrode was washed with PC and diethyl carbonate (Kishida Chemical Co., Ltd.). The electrode surface was observed before and after charge-discharge testing by field emission

scanning electron microscopy (FE-SEM; JSM-6701F, JEOL Co., Ltd.). The acceleration voltage and working distance were set at 3 kV and 8 mm, respectively. The root-mean-square roughness (Sq) of the electrode surface was estimated by confocal laser scanning microscopy (CLSM, VK-9700, Keyence). The cross-sectional observation was conducted by FE-SEM (JSM-7800F, JEOL Co., Ltd.). The electrode was not exposed to the atmosphere until it was introduced into the chamber of the FE-SEM using a transfer vessel. The acceleration voltage and working distance were set at 5 kV and 10 mm, respectively. A cross-section polisher (CP; IB09020CP, JEOL Co., Ltd.) was used to fabricate the cross-sectional surface.

3. Results and Discussion

Characterization of $FeSi_2$/Si Composite. —— Figure 1a shows XRD pattern of $FeSi_2$/Si (56/44 wt.%) composite powder. The Inorganic Crystal Standard Database (ISCD) pattern of Si, $FeSi_2$, and FeSi is also shown. Only peaks assigned to Si and $FeSi_2$ were confirmed. There were no peaks assigned to FeSi; an impurity did not form. Because the size of pristine $FeSi_2$/Si particle was relatively large, the GD electrode could not be prepared as received. Hence, we reduced the particle size by mechanical grinding (MG). Figure 1b and 1c displays particle size distribution of $FeSi_2$/Si (56/44 wt.%) composite powder before and after MG. The average particle size reduced from 70 to 7 μm by MG. We prepared the GD electrode using the ground $FeSi_2$/Si powder.

Cycle Life of $FeSi_2$/Si Composite Electrodes. —— Figure S2 shows cycling performance of $FeSi_2$/Si (56/44 wt.%) composite electrode in various electrolytes. To discuss the difference of electrochemical performance easily, we performed charge-discharge testing with a charge capacity limit of 1000 mA h g(Si)$^{-1}$ (Figures 2 and S3). Figure S3 shows the first, fifth, 10th and 60th charge-discharge curve of $FeSi_2$/Si (56/44 wt.%) composite electrode with a charge capacity limit of 1000 mA h g(Si)$^{-1}$ in various electrolytes. As mentioned above, we can see that the discharge capacity did not reach 1000 mA h g(Si)$^{-1}$ during the initial 10 cycles in all electrolytes (Figure S3a–S3c). At the 60th cycle, similar charge-discharge behavior was observed not depending used electrolyte. Figure 2 displays the cycle life of $FeSi_2$/Si (56/44 wt.%) composite electrode with a charge capacity limit of 1000 mA h g(Si)$^{-1}$ in various electrolytes. The discharge capacity did not reach 1000 mA h g(Si)$^{-1}$ during the initial 10 cycles in all electrolytes. In the organic-liquid electrolytes (LiTFSA/PC and LiFSA/PC), the reversible capacity decayed at around the 100th cycle irrespective of Li salt and the Coulombic efficiency (CE) drops at almost the same cycle (at around the 60th cycle). It is well-known that the surface film is formed through reductive decomposition of the electrolyte. A large volumetric change in the Si during charge-discharge reactions leads to cracking and pulverization of the active material layer as well as collapsing of the resulting film. The CE drop indicates the reconstitution of the surface film on the newly formed Si surface. We have previously reported that a surface film with an uneven thickness forms on the surface of Si-based electrode in an organic-liquid electrolyte and Li^+ is preferentially stored into the electrode via the thinner parts of the film, which causes local change in the Si volume and the electrode

disintegration.[8,41] Because similar phenomena would occur on the $FeSi_2$/Si electrode, the reversible capacity faded relatively early.

On the other hand, in the ionic-liquid electrolytes (LiFSA/EMI-FSA and LiFSA/Py13-FSA), the $FeSi_2$/Si electrode maintained a reversible capacity of 1000 mA h g$(Si)^{-1}$ over 550 and 850 cycles, respectively. Because the FSA anion decomposes very rapidly to form a surface film including LiF which contributes to its structural and/or mechanical stability,[50] it is considered that growth of the surface film was suppressed and the film remained thin and uniform. This indicates that homogeneous lithiation on the entire electrode surface takes place, preventing the occurrence of local stress. Thus, severe $FeSi_2$/Si electrode disintegration, which causes capacity fading, is suppressed. The initial CE in both ionic-liquid electrolytes was very low (Figure S3a), whereas this reaches approximately 99% after the 60th cycle without drop (Figure S3d). This result indicates that the active material layer does not disintegrate in the ionic-liquid electrolytes. It is considered that lower CE in the EMI-based electrolyte is attributed to continuing reductive decomposition of the EMI cation at ca. 0.6 V vs. Li^+/Li to form a surface film (Figure S3b and S3c).[51,52] Although the charge potential did not approach 0.6 V vs. Li^+/Li in Figure S3a, this is because FSA anion decomposes at approximately 1.5 V vs Li^+/Li. As a result, the surface film derived from the EMI-based electrolyte was thicker than that derived from the Py13-based electrolyte. Hence, we concluded that the $FeSi_2$/Si electrode exhibits longer cycle life in the Py13-based electrolyte.

Figure S4 shows cycle life of $FeSi_2$/Si (42/58 wt.%) composite electrode with different composition from foregoing electrode in 1 M LiFSA/Py13-FSA with a charge capacity limit of 1000 mA h g^{-1}. For comparison, the result of $FeSi_2$/Si (56/44 wt.%) and Si-alone electrodes is also shown. While

both composite electrodes exhibited longer cycle life than Si-alone electrode, such difference in the mixing ratio of $FeSi_2$ and Si did not influence on the cycle life.

Change in Surface Morphology and Thickness. —— To determine the difference between the cycle lives of the $FeSi_2$/Si (56/44 wt.%) composite electrode in various electrolytes, we observed change in the surface morphology of the electrode at the 100th cycle by FE-SEM (Figure 3). In the organic-liquid electrolytes, there were large cracks on the electrode surface. Additionally, the Sq value increased more than threefold compared to that before charge-discharge testing. Conversely, in the ionic-liquid electrolytes, the surface morphology was almost the same as that before cycling, even though fine cracks formed. An increase in the Sq was slight.

Figure 4 displays cross-sectional SEM images of the $FeSi_2$/Si (56/44 wt.%) composite electrode. The thickness of nonlithiated $FeSi_2$/Si active material layer before charge-discharge testing was 2.7 ± 0.4 μm. In the 1 M LiFSA/PC, the thickness of active material layer increased to 11.2 ± 1.9 μm after the 100th cycle when the discharge capacity faded. On the other hand, an increase in the thickness was suppressed in the 1 M LiFSA/Py13-FSA (5.4 ± 1.3 μm). Consequently, better cycle life in the ionic-liquid electrolytes should be attributed to suppression of crack formation and active material expansion.

Rate Performance of $FeSi_2$/Si Composite Electrodes. —— Figure 5 shows rate performance of the $FeSi_2$/Si (56/44 wt.%) composite electrode in various electrolytes with a charge capacity limit of 1000 mA h g^{-1}. The electrode retained a discharge capacity of 1000 mA h g^{-1} up to 5*C* in all electrolytes,

whereas the capacity faded at 10C in the electrolytes other than LiFSA/EMI-FSA: the composite electrode maintained the capacity of 1000 mA h g^{-1} in only LiFSA/EMI-FSA. Figure S5 shows Nyquist plot of $FeSi_2$/Si (56/44 wt.%) composite electrode in 1 M LiFSA/EMI-FSA and 1 M LiFSA/Py13-FSA. There was no significant difference in resistance of solution, charge transfer, and surface film at high and middle frequency ranges regardless of the electrolyte. In contrast, Li^+ diffusion in the electrolyte at low frequency region clearly differed. Ionic conductivity of LiFSA/EMI-FSA, LiFSA/Py13-FSA, LiFSA/PC, and LiTFSA/PC is 12.3, 5.4, 6.8, and 5.6 mS cm^{-1}, respectively: the excellent rate capability was obtained in the EMI-based electrolyte with high ionic conductivity since the Li^+ diffusion in the electrolyte is dominant at high *C*-rates. [46] Additionally, it has been reported that the decomposition of EMI-FSA results in a large number of inorganic compounds including LiOH and Li_2O, which leads to a superior rate capability of Si-based electrodes in the electrolyte.[53]

Figure 6 provides rate capability of $FeSi_2$/Si (42/58 wt.%), $FeSi_2$/Si (56/44 wt.%), and Si-alone electrodes in 1 M LiFSA/EMI-FSA with a charge capacity limit of 1000 mA h $g(Si)^{-1}$. Being different from Figure 5, Figure 6 was obtained after pre-cycling.[47] Thus, the initial discharge capacities in Figure 6 were close to 1000 mA h g^{-1}. The Si-alone electrode showed a capacity fading at 10*C* and little capacity at 50*C*. Rate performance of both $FeSi_2$/Si composite electrodes was superior to that of the Si-alone electrode, which is arising from high electron conductivity of $FeSi_2$: current collecting property of Si electrode was improved due to $FeSi_2$. Additionally, the $FeSi_2$/Si (56/44 wt.%) electrode exhibited a superior performance to $FeSi_2$/Si (42/58 wt.%) electrode, which is attributed to its higher $FeSi_2$ content.

Electrochemical Performance under Adjusted Conditions. —— We have previously reported that a $FeSi_2$-alone electrode shows low discharge capacity of approximately 60 mA h g^{-1} with significant cycle stability in a PC-based organic-liquid electrolyte at high current density (blue plot in Figure S6).[21] We have also found that the electrode exhibits more than 10 times higher initial capacities in a similar electrolyte at low current density (50 mA g^{-1}), whereas the capacity rapidly faded (black plot in Figure S6).[45] On the other hand, the electrode has shown excellent cycle stability with high reversible capacity of ca. 630 mA h g^{-1} in the Py13-based ionic-liquid electrolyte at low current density (red plot in Figure S6).[45] These results demonstrate that $FeSi_2$-alone electrode has charge-discharge capacity in the ionic-liquid electrolyte, while above results (Figures 2, 5, and 6) have obtained assuming that the capacity of $FeSi_2$ is very low. Hence, we adjusted *C*-rate and charge capacity limit value of $FeSi_2$ electrode and standardized these conditions to discuss difference in the electrochemical performance between electrodes. Table 1 summaries the adjusted charge-discharge conditions.

Figure 7 provides cycle life of various electrodes in 1 M LiFSA/Py13-FSA with the adjusted conditions. Vertical axis presents utilization rate of active materials which is calculated according to equation shown in Figure 7. In the present study, the utilization rate was set at 28% which corresponds to capacity limit of 1000 mA h g^{-1} for a Si-alone electrode. $FeSi_2$-alone electrode showed the longest cycle life and its utilization rate decreased at around the 3500th cycle (data not shown). We expected that the $FeSi_2$/Si (56/44 wt.%) composite electrode shows longer cycle life compared to the Si-alone electrode because $FeSi_2$ covers the shortcoming of Si as mentioned in introduction section. However, the

utilization rate of the $FeSi_2$/Si (56/44 wt.%) and Si-alone electrodes decayed at almost the same cycle (670th cycle).

To discuss above unpredictable result, we confirmed the 10th charge-discharge curve (Figure 8). The $FeSi_2$ electrode exhibited the potential slope between 0.9 and 0.3 V vs. Li^+/Li on charge curve, which is attributed to lithiation reaction of $FeSi_2$. In contrast, the potential plateau was observed at around 0.2 V vs. Li^+/Li on charge curve of Si.[44] This plateau is assigned to alloying of Si with Li. Although we expected that the $FeSi_2$/Si (56/44 wt.%) composite electrode exhibits blue dotted profile, the electrode showed the charge-discharge curve similar to that of the Si-alone electrode not depending on *C*-rate. This result demonstrated that Li was stored only in Si of $FeSi_2$/Si composite electrode. Remarkably, only Si of $FeSi_2$/Si composite electrode alloys with Li whereas each $FeSi_2$- and Si-alone electrode alloys with Li in the ionic-liquid electrolyte. In other words, $FeSi_2$ in $FeSi_2$/Si composite electrode should play no role of active material. Similar profiles were also obtained after long cycle, as shown in Figure S7. The reason why no Li^+ is stored in $FeSi_2$ of $FeSi_2$/Si composite electrode is under study.

In such cases, the *C*-rate and utilization rate of active materials must be higher than those described in Table 1. Based on ratio by weight (56/44 wt.%) in $FeSi_2$/Si composite electrode, we recalculated the *C*-rate and utilization rate of active materials, as shown in Table 2. Although the utilization rate of active materials decreases under high *C*-rate, the rate of Si in $FeSi_2$/Si (56/44 wt.%) composite electrode increased. This is because the current collecting property of $FeSi_2$/Si composite electrode is superior due to high electronic conductivity of $FeSi_2$. Additionally, massive volume change in Si often occurs under higher utilization rate of active materials, which leads to lowering of the cycle

life. However, the life of $FeSi_2$/Si (56/44 wt.%) composite electrode was equal to that of Si-alone electrode (Figure 7). It is considered that $FeSi_2$ releases the stress generating from Si

Figure 9 shows rate capability of various electrodes in 1 M LiFSA/EMI-FSA with conditions of Table 1. While the utilization rate of active materials of $FeSi_2$/Si (56/44 wt.%) composite electrode was higher than that of Si-alone electrode (Figure 8, Table 2), the composite electrode exhibited a superior rate performance compared to Si-alone electrode, which results from low electric resistivity of $FeSi_2$.[21] Additionally, mechanical properties suitable for relaxation of the stress generating from Si and/or moderate reactivity with Li^+ of $FeSi_2$ would be attributed to the improvement in high-rate performance.

4. Conclusion

We investigated the electrochemical performance of $FeSi_2$/Si composite electrode in various electrolytes. In the PC-based organic-liquid electrolytes, the electrode showed poor cycle life with a discharge capacity of 1000 mA h g$(Si)^{-1}$ until the 100th cycle irrespective of Li salt. On the other hand, in the Py13-based ionic-liquid electrolyte, the $FeSi_2$/Si electrode exhibited a superior cycle life with a reversible capacity of 1000 mA h g$(Si)^{-1}$ over 850 cycles. SEM observations revealed that difference in the cycle life is determined by surface film properties. Additionally, the electrode showed an improved rate capability in the EMI-based ionic-liquid electrolyte. Interestingly, only lithiation of Si in $FeSi_2$/Si composite electrode occurred in the ionic-liquid electrolyte irrespective of *C*-rate whereas each $FeSi_2$- and Si-alone electrode alloyed with Li: $FeSi_2$ in $FeSi_2$/Si composite electrode plays no role of active

material. $FeSi_2$ certainly covered the shortcomings of Si and the $FeSi_2$/Si composite electrode exhibited improved cycle life and rate capability compared to Si-alone electrode.

Supporting Information: The Supporting Information is available on the website at DOI: xxxxxxxxxxxxx.

Acknowledgement

This work was partially supported by the Japan Society for the Promotion of Science (JSPS) KAKENHI (Grant numbers 19K05649, 19H02817, JP20H00399, and JP18K04965) and the NIMS Joint Research Hub Program.

References

1. S.-C. Lai, *J. Electrochem. Soc.,* **123**, 1196 (1976).

2. M. N. Obrovac and L. Christensen, *Electrochem. Solid-State Lett*., **7**, A93 (2004).

3. M. N. Obrovac and L. J. Krause, *J. Electrochem. Soc*., **154**, A103 (2007).

4. B. Key, M. Morcrette, J.-M. Tarascon, and C. P. Grey, *J. Am. Chem. Soc*., **133**, 503 (2011).

5. X. H. Liu, L. Zhong, S. Huang, S. X. Mao, T. Zhu, and J. Y. Huang, *ACS Nano*, **6**, 1522 (2012).

6. N. Ding, J. Xu, Y. X. Yao, G. Wegner, X. Fang, C. H. Chen, and I. Lieberwirth, *Solid State Ionics*, **180** 222 (2009).

7. J. Xie, N. Imanishi, T. Zhang, A. Hirano, Y. Takeda, and O. Yamamoto, *Mater. Chem. Phys*., **120**, 421 (2010).

8. Y. Domi, H. Usui, K. Yamaguchi, S. Yodoya, and H. Sakaguchi, *ACS Appl. Mater. Interfaces*, **11**, 2950 (2019).

9. X. Zhou, Y.-X. Yin, A.-M. Cao, L.-J. Wan, and Y.-G. Guo, *ACS Appl. Mater. Interfaces*, **4**, 2824 (2012).

10. G. D. Park, J. H. Choi, D. S. Jung, J.-S. Park, and Y. C. Kang, *J. Alloys Compds*., **821**, 153224 (2020).

11. C. Jo, A. S. Groombridge, J. D. L. Verpilliere, J. T. Lee, Y. Son, H.-L. Liang, A. M. Boies, and M. D. Volder, *ACS Nano*, **14**, 698 (2020).

12. M. T. McDowell, I. Ryu, S. W. Lee, C. Wang, W. D. Nix, and Y. Cui, *Adv. Mater.*, **24**, 6034 (2012).

13. B. Liu, X. Wang, H. Chen, Z. Wang, D. Chen, Y.-B. Cheng, C. Zhou, and G. Shen, *Sci. Rep*., **3**, 1622 (2013).

14. X. Zhou, L.-J. Wan, and Y.-G. Guo, *Small*, **9**, 2684 (2013).

15. Y. Domi, H. Usui, D. Iwanari, and H. Sakaguchi, *J. Electrochem. Soc*., **162**, A1651 (2017).

16. M. Saito, K. Kato, S. Ishii, K. Yoshii, M. Shikano, H. Sakaebe, H. Kikuchi, T. Fukunaga, and E. Matsubara, *J. Electrochem. Soc*., **166**, A5174 (2019).

17. B. R. Long, M. K. Y. Chan, J. P. Greeley, and A. A. Gewirth, *J. Phys. Chem. C*, **115**, 18916 (2011).

18. R. Yi, J. Zai, F. Dai, M. L. Gordin, and D. Wang, *Electrochem. Commun*., **36**, 29 (2013).

19. Y. Domi, H. Usui, M. Shimizu, Y. Kakimoto, and H. Sakaguchi, *ACS Appl. Mater. Interfaces*, **8**, 7125 (2016).

20. H. Usui, K. Maebara, K. Nakai, and H. Sakaguchi, *Int. J. Electrochem. Sci*., **6**, 2246 (2011).

21. H. Usui, K. Nouno, Y. Takemoto, K. Nakada, A. Ishii, and H. Sakaguchi, *J. Power Sources*, **268**, 848 (2014).

22. H. Usui, M, Nomura, H. Nishino, M. Kusatsu, T. Murota, and H. Sakaguchi, *Mater. Lett.*, **130**, 61 (2014).

23. Y. Domi, H. Usui, Y. Takemoto, K. Yamaguchi, and H. Sakaguchi, *Chem. Lett*., **45**, 1198 (2016).

24. Y. Domi, H. Usui, Y. Takemoto, K. Yamaguchi, and H. Sakaguchi, *J. Phys. Chem. C*, **120**, 16333 (2016).

25. T. Iida, T. Hirono, N. Shibamura, and H. Sakaguchi, *Electrochemistry*, **76**, 644 (2008).

26. H. Sakaguchi, T. Iida, M. Itoh, N. Shibamura, and T. Hirono, *IOP Conf. Series: Mater. Sci. Eng*., **1**, 012030 (2009).

27. J. Wang, Y. Yamada, K. Sodeyama, C. H. Chiang, Y. Tateyama, and A. Yamada, *Nat. Commun*., **7**, 12032 (2016).

28. K. Matsumoto, J. Hwang, S. Kaushik, C.-Y. Chen, and R. Hagiwara, *Energy Environ. Sci*., **12**, 3247 (2019).

29. K. Yamaguchi, Y. Domi, H. Usui, M. Shimizu, S. Morishita, S. Yodoya, T. Sakata, and H. Sakaguchi, *J. Electrochem. Soc*., **166**, A268 (2019).

30. Y. Domi, H. Usui, E. Nakabayashi, T. Yamamoto, T. Nohira, and H. Sakaguchi, *Electrochemistry*, **87**, 333 (2019).

31. T. Yamamoto and T. Nohira, *Chem. Commun*., **56**, 2538 (2020).

32. H. Qi, Y. Ren, S. Guo, Y. Wang, S. Li, Y. Hu, and F. Yan, *ACS Appl. Mater. Interfaces*, **12**, 591 (2020).

33. M. Shimizu, K. Yamaguchi, H. Usui, N. Ieuji, T. Yamashita, T. Komura, Y. Domi, T. Nokami, T. Itoh, and H. Sakaguchi, *J. Electrochem. Soc*., **167**, 070516 (2020).

34. T. Achiha, T. Nakajima, Y. Ohzawa, M. Koh, A. Yamauchi, M. Kagawa, and H. Aoyama, *J. Electrochem. Soc*., **156**, A483 (2009).

35. H. Nakagawa, Y. Shibata, Y. Fujino, T. Tabuchi, T. Inamasu, and T. Murata, *Electrochemistry*, **78**, 406 (2010).

36. H. Nakagawa, M. Ochida, Y. Domi, T. Doi, S. Tsubouchi, T. Yamanaka, T. Abe, and Z. Ogumi, *J. Power Sources*, **212**, 148 (2012).

37. M. J. Earle, J. M. S. S. Esperança, M. A. Gilea, J. N. C. Lopes, L. P. N. Rebelo, J. W. Magee, K. R. Seddon, and J. A. Widegren, *Nature*, **439**, 831 (2006).

38. P. Hapiot and C. Lagrost, *Chem. Rev*., **108**, 2238 (2008).

39. P. Sippel, P. Lunkenheimer, S. Krohns, R. Thoms, and A. Loidl, *Sci. Rep*., **5**, 13922 (2015).

40. A. Ghoufi, A. Szymcxyk, and P. Malfreyt, *Sci. Rep*., **6**, 28518 (2016).

41. M. Shimizu, H. Usui, T. Suzumura, and H. Sakaguchi, *J. Phys. Chem. C*, **119**, 2975 (2015).

42. Y. Domi, H. Usui, M. Narita, Y. Fujita, K. Yamaguchi, and H. Sakaguchi, *J. Electrochem. Soc*., **164**, A3208 (2017).

43. K. Yamaguchi, Y. Domi, H. Usui, M. Shimizu, K. Matsumoto, T. Nokami, T. Itoh, and H. Sakaguchi, *J. Power Sources*, **338**, 103 (2017).

44. K. Yamaguchi, Y. Domi, H. Usui, and H. Sakaguchi, *ChemElectroChem*, **4**, 3257 (2017).

45. Y. Domi, H. Usui, R. Takaishi, and H. Sakaguchi, *ChemElectroChem*, **6**, 581 (2019).

46. S. Yodoya, Y. Domi, H. Usui, and H. Sakaguchi, *ChemistrySelect*, **4**, 1375 (2019).

47. Y. Domi, H. Usui, A. Ueno, Y. Shindo, H. Mizuguchi, T. Komura, T. Nokami, T. Itoh, and H. Sakaguchi, *J. Electrochem. Soc*., **167**, 040512 (2020).

48. M. Shimizu, H. Usui, K. Matsumoto, T. Nokami, T. Itoh, and H. Sakaguchi, *J. Electrochem. Soc.*, **161**, A1765 (2014).

49. Y. Domi, H. Usui, M. Shimizu, K. Miwa, and H. Sakaguchi, *Int. J. Electrochem. Sci*., **10**, 9678 (2015).

50. D. M. Piper, T. Evans, K. Leung, T. Watkins, J. Olson, S. C. Kim, S. S. Han, V. Bhat, K. H. Oh, D. A. Buttry, and S.-H. Lee, *Nat. Commun*., **6**, 7230 (2015).

51. T. Sugimoto, M. Kikuta, E. Ishiko, M. Kono, and M. Ishikawa, *J. Power Sources*, **183**, 436 (2008).

52. T. Sugimoto, Y. Atsumi, M. Kono, M. Kikuta, E. Ishiko, M. Yamagata, and M. Ishikawa, *J. Power Sources*, **195**, 6153 (2010).

53. H. Shobukawa, J. Shin, J. Alvarado, C. S. Rustomji, and Y. S. Meng, *J. Mater. Chem. A*, **4**, 15117 (2016).

54. C.-C. Nguyen, S.-W. Woo, and S.-W. Song, *J. Phys. Chem. C*, **116**, 14764 (2012).

Table 1. Adjusted current density and charge capacity limit value.

	Si	$FeSi_2$	$FeSi_2$/Si (56/44 wt.%)
Current density	3.6 A g^{-1}	0.63 A g^{-1}	1.94 A g^{-1}
(*C*-rate)	(1.0*C*)	(1.0*C*)	(1.0*C*)
Charge capacity limit	1000 mA h g^{-1}	175 mA h g^{-1}	538 mA h g^{-1}
(Utilization rate)	(28%)	(28%)	(28%)
Theoretical (maximum) capacity	3600 mA h g^{-1}	630 mA h g^{-1}	1937 mA h g^{-1}

Table 2. Recalculated *C*-rate and utilization rate of active materials.

	$FeSi_2$/Si (56/44 wt.%)[#]	$FeSi_2$/Si (56/44 wt.%)[‖]
C-rate	1.0*C*	2.3C
Utilization rate	28%	63%

[#] Assuming that both $FeSi_2$ and Si alloy with Li, we calculated.

[‖] Based on the fact that only Si in $FeSi_2$/Si composite electrode alloys with Li, we calculated.

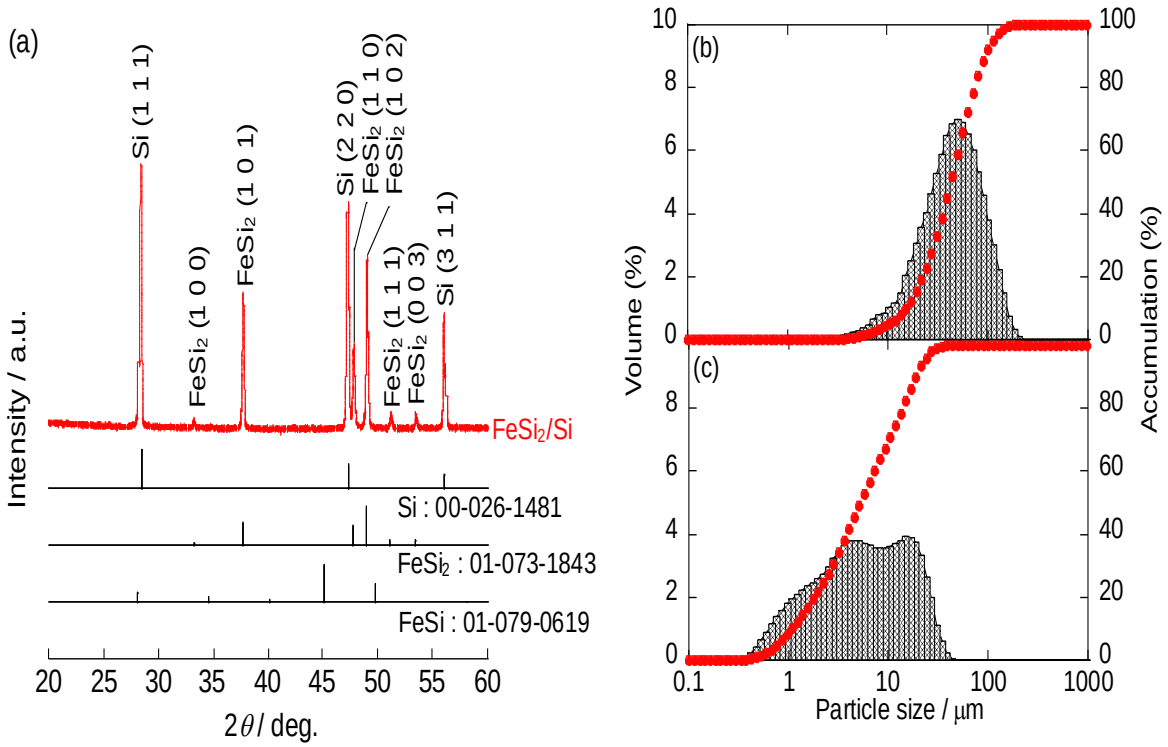

Figure 1. (a) XRD patterns of $FeSi_2$/Si (56/44 wt.%) composite powder and its particle size distribution (b) before and (c) after MG.

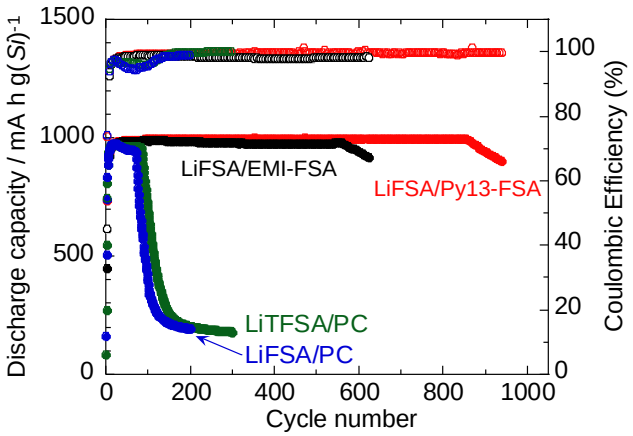

Figure 2. Cycle life of $FeSi_2$/Si (56/44 wt.%) composite electrode in various electrolytes with a charge capacity limit of 1000 mA h g$(Si)^{-1}$. The current density was set at 0.1C during the first cycle and 0.4C during the subsequent cycles.

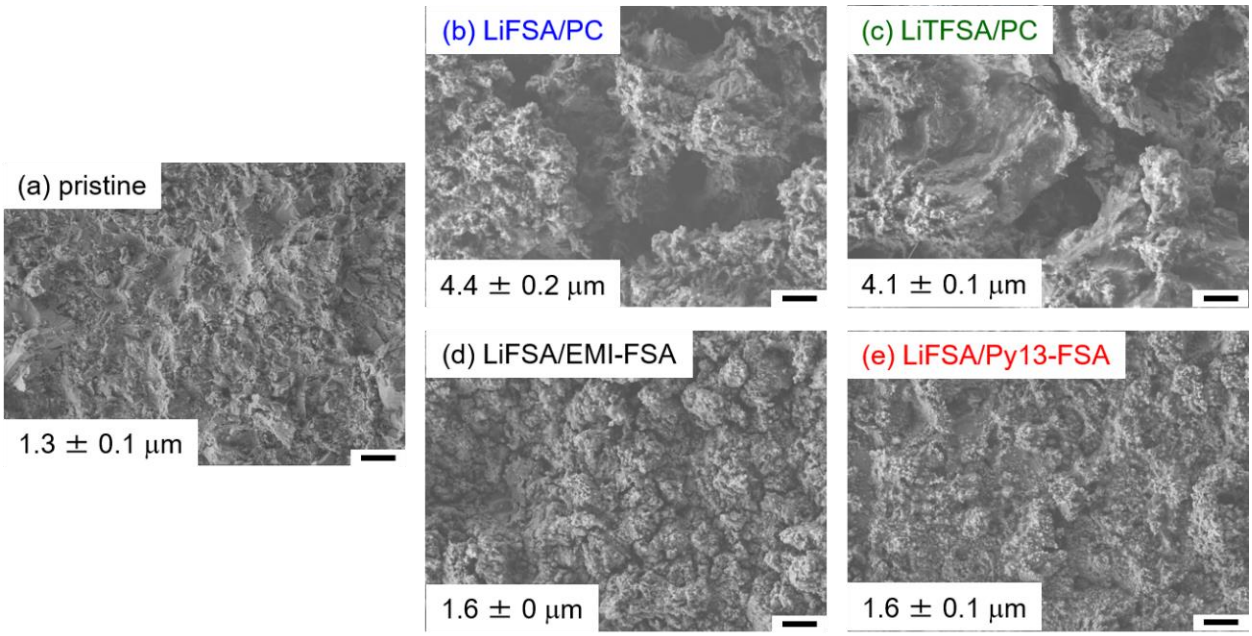

Figure 3. SEM images of $FeSi_2$/Si (56/44 wt.%) electrode surface (a) before and (b–e)after 100th cycle with a charge capacity limit of 1000 mA h g$(Si)^{-1}$ in (b) LiFSA/PC (c) LiTFSA/PC, (d) LiFSA/EMI-FSA, and (e) LiFSA/Py13-FSA. The scale bar represents 2 μm. Average Sq of the electrode surface estimated by CLSM is shown with a standard deviation at the lower left in each part. The standard deviation of Sq in part (d) was below 0.1 μm.

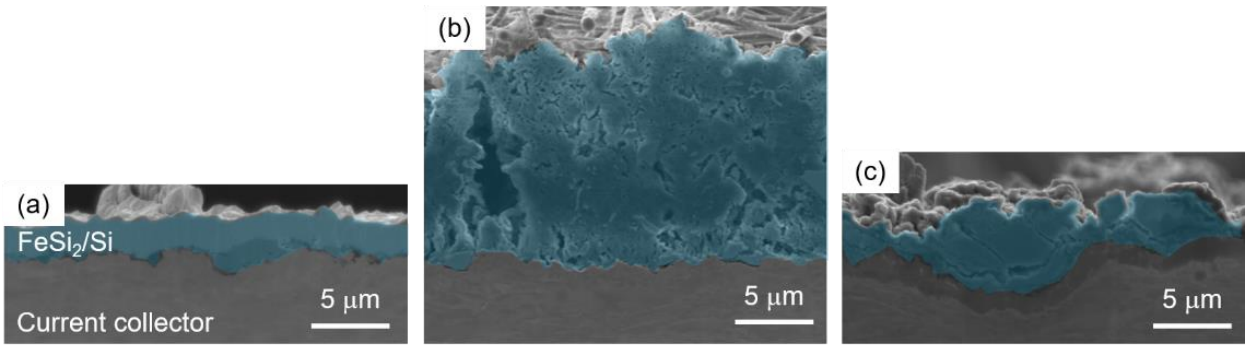

Figure 4. Cross-sectional SEM images of $FeSi_2$/Si (56/44 wt.%) electrode (a) before and (b and c) after the 100th cycle with a charge capacity limit of 1000 mA h g$(Si)^{-1}$ in (b) LiFSA/PC and (c) LiFSA/Py13-FSA. Each blue-colored area indicates $FeSi_2$/Si active material layer.

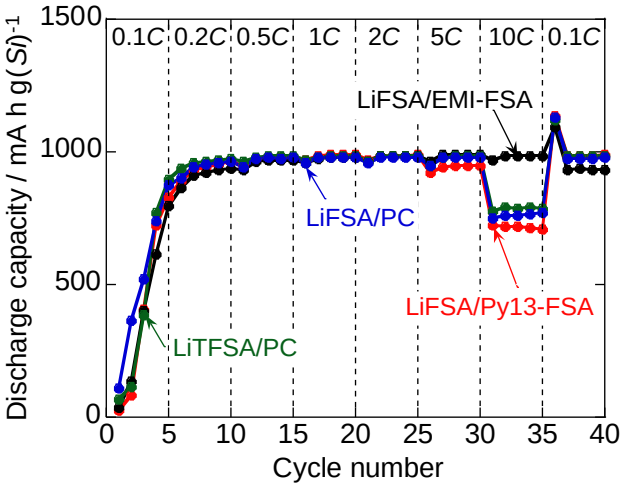

Figure 5. Rate performance of $FeSi_2$/Si (56/44 wt.%) composite electrode in various electrolytes with a charge capacity limit of 1000 mA h g$(Si)^{-1}$.

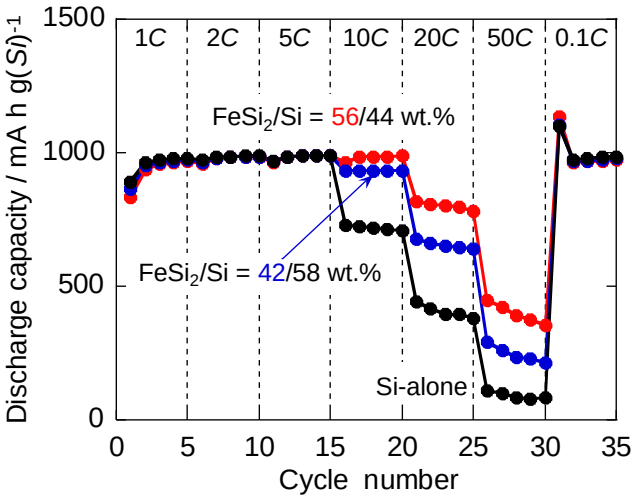

Figure 6. Rate capability of $FeSi_2$/Si (42/58 wt.%), $FeSi_2$/Si (56/44 wt.%), and Si-alone electrodes in 1 M LiFSA/EMI-FSA with a charge capacity limit of 1000 mA h g^{-1}.

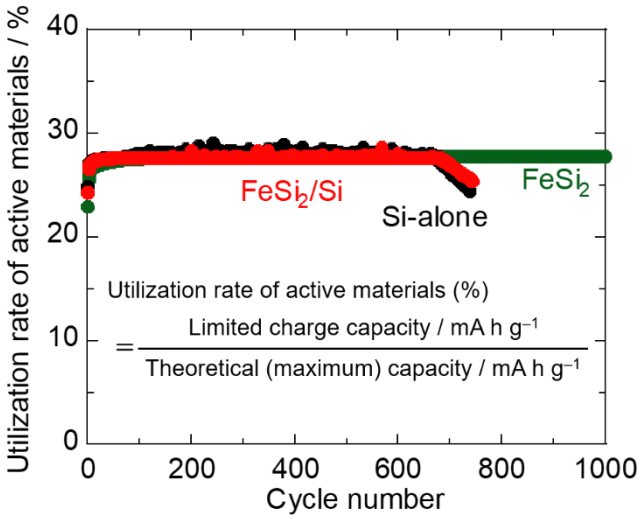

Figure 7. Cycle life of $FeSi_2$/Si (56/44 wt.%), Si, and $FeSi_2$ electrodes in 1 M LiFSA/Py13-FSA at 1*C*. Vertical axis is utilization rate of active materials, which is divided limited charge capacity by theoretical (maximum) capacity. The unit mass in each capacity is based on active material unlike that in Figures 2, 5, and 6.

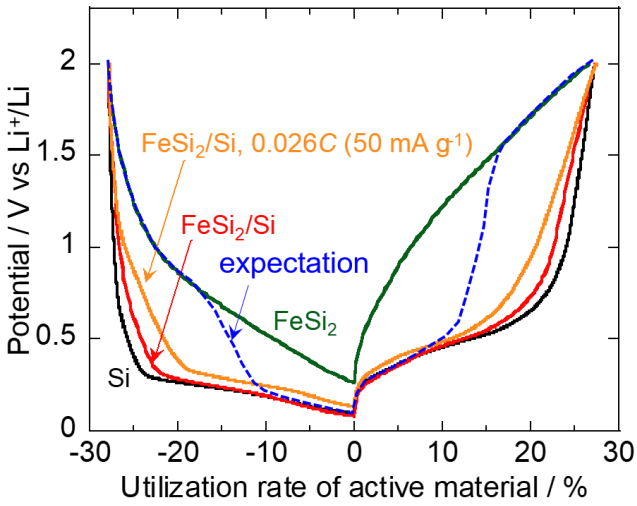

Figure 8. 10th charge-discharge curve of $FeSi_2$/Si (56/44 wt.%), Si, and $FeSi_2$ electrodes in 1 M LiFSA/Py13-FSA at 1*C*. Horizontal axis is utilization rate of active materials. Blue dotted line denotes expected charge-discharge profile.

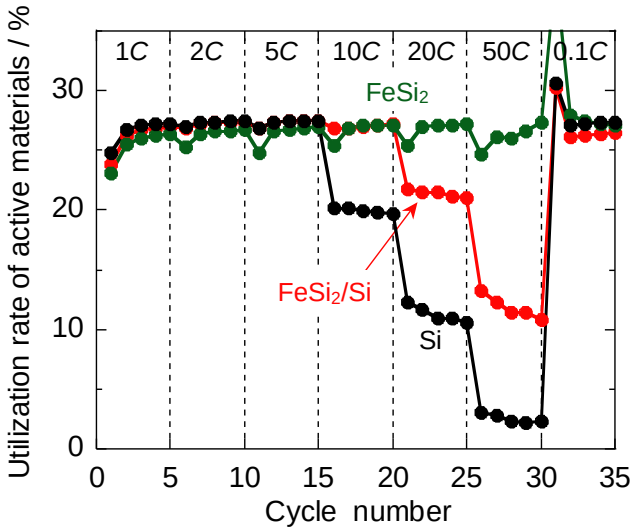

Figure 9. Rate performance of $FeSi_2$/Si (56/44 wt.%), Si, and $FeSi_2$ electrodes in 1 M LiFSA/EMI-FSA. Vertical axis is utilization rate of active material, and the rate was set at 28%.

Figure Captions

Table 1. Adjusted current density and charge capacity limit value.

Table 2. Recalculated *C*-rate and utilization rate of active materials.

Figure 1. (a) XRD patterns of $FeSi_2$/Si (56/44 wt.%) composite supplied from Elkem. Particle size distribution of $FeSi_2$/Si (56/44 wt.%) composite powders (b) before and (c) after MG.

Figure 2. Cycle life of $FeSi_2$/Si (56/44 wt.%) composite electrode in various electrolytes with a charge capacity limit of 1000 mA h g$(Si)^{-1}$. The current density was set at 0.1*C* during the first cycle and 0.4*C* during the subsequent cycles.

Figure 3. SEM images of $FeSi_2$/Si (56/44 wt.%) electrode surface (a) before and (b–e)after 100th cycle with a charge capacity limit of 1000 mA h g$(Si)^{-1}$ in (b) LiFSA/PC (c) LiTFSA/PC, (d) LiFSA/EMI-FSA, and (e) LiFSA/Py13-FSA. The scale bar represents 2 μm. Average Sq of the electrode surface estimated by CLSM is shown with a standard deviation at the lower left in each part. The standard deviation of Sq in part (d) was below 0.1 μm.

Figure 4. Cross-sectional SEM images of $FeSi_2$/Si (56/44 wt.%) electrode (a) before and (b and c) after the 100th cycle with a charge capacity limit of 1000 mA h g(Si)$^{-1}$ in (b) LiFSA/PC (c) LiFSA/Py13-FSA. Each blue-colored area indicates $FeSi_2$/Si active material layer.

Figure 5. Rate performance of $FeSi_2$/Si (56/44 wt.%) composite electrode in various electrolytes with a charge capacity limit of 1000 mA h g(Si)$^{-1}$.

Figure 6. Rate capability of $FeSi_2$/Si (42/58 wt.%), $FeSi_2$/Si (56/44 wt.%), and Si-alone electrodes in 1 M LiFSA/EMI-FSA with a charge capacity limit of 1000 mA h g^{-1}.

Figure 7. Cycle life of $FeSi_2$/Si (56/44 wt.%), Si, and $FeSi_2$ electrodes in 1 M LiFSA/Py13-FSA at 1C. Vertical axis is utilization rate of active materials, which is divided limited charge capacity by theoretical (maximum) capacity. The unit mass in each capacity is based on active material unlike that in Figures 2, 5, and 6.

Figure 8. 10th charge-discharge curve of $FeSi_2$/Si (56/44 wt.%), Si, and $FeSi_2$ electrodes in 1 M LiFSA/Py13-FSA at 1C. Horizontal axis is utilization rate of active materials. Blue dotted line denotes expected charge-discharge profile.

Figure 9. Rate performance of $FeSi_2$/Si (56/44 wt.%), Si, and $FeSi_2$ electrodes in 1 M LiFSA/EMI-FSA. Vertical axis is utilization rate of active material, and the rate was set at 28%.